XAFS analysis on amorphous and crystalline new phase change material $GeCu_2Te_3$

K. KAMIMURA[a], S. HOSOKAWA[*,a], N. HAPPO[b], H. IKEMOTO[c], Y. SUTOU[d], S. SHINDO[d], Y. SAITO[d], J. KOIKE[d]
[a]*Department of Physics, Graduate School of Science and Technology, Kumamoto University, Kumamoto 860-8555, Japan*
[b]*Department of Frontier Sciences, Graduate School of Information Sciences, Hiroshima City University, Hiroshima 731-3194, Japan*
[c]*Department of Physics, Faculty of Science, University of Toyama, Toyama 930-8555, Japan*
[d]*Department of Materials Science, Graduate School of Engineering, Tohoku University, Sendai, 980-8579, Japan*

The structure of crystalline and amorphous $GeCu_2Te_3$ phase change material was investigated by x-ray absorption fine structure. The averaged interatomic distances of Ge-Te and Cu-Te in the crystal phase are confirmed to contradict the x-ray diffraction data, and are mostly equal to the experimental data in the amorphous phase. As regards the coordination numbers, the atomic configurations around the Ge atoms are a small modification of the crystalline one, while those around the Cu atoms are quite different and the large number of the Cu-Cu homopolar coordination become an important role in the amorphous phase. The x-ray absorption near edge structure data near the Ge *K* edge show a similarity of the local atomic configurations around the Ge atoms between the crystalline and amorphous $GeCu_2Te_3$. However, those near the Cu *K* edge indicate a large smearing-out on the amorphization, corresponding the large differences in the atomic configurations around the Cu atoms.

(Received November 05, 2015; accepted April 05, 2016)

Keywords: Phase change material, Local structure, XAFS

1. Introduction

$Ge_2Sb_2Te_5$ (GST) has intensively been studied for the use of phase change random access memory (PCRAM) because of the fast phase-change speed and the good reversibility between amorphous and crystalline states [1]. PCRAM is operated by Joule heating to induce a phase transition between a high-resistance amorphous phase (reset state) and a low-resistance crystalline phase (set state) of a phase change material (PCM) [2]. The melting temperature, T_m, of GST is over 600°C, indicating that a high power consumption is required for its reset operation, while the crystallization temperature, T_c, is about 150°C, limiting its data retention capability [3]. To improve the quality of PCMs, a higher T_c and a lower T_m are necessary.

The T_c value of a new PCM, $GeCu_2Te_3$ (GCT), discovered by Sutou *et al.* [4], is about 250°C, while T_m is about 500°C. The phase change of GCT rapidly occurs within some 10 ns [5]. Therefore, GCT is a promising PCM with a low power consumption, an excellent data retention, and a high-speed rewriting operation [6]. For the understandings of the fast phase change mechanism, it is important to know the local structures on both the phases.

Fig. 1 shows the structure of crystalline GCT obtained by x-ray diffraction (XRD) [7]. The crystal has a Cu_2GeSe_3-type orthorhombic structure with a space group of Imm2. In this structure, crystalline GCT is built up of corner-sharing $GeTe_4$ and $CuTe_4$ tetrahedrons. We have recently investigated the local structure of crystalline GCT using x-ray absorption fine structure (XAFS) technique [8].

The averaged interatomic distance R_{ij} in crystalline GCT obtained from XRD [7] and XAFS [8] measurements are tabulated in Table 1 together with R_{ij} in amorphous GCT obtained from XAFS [9]. We surprisingly found that compared with the XRD results, the average Ge-Te interatomic distance is larger, and the Cu-Te one is smaller. Moreover, the averaged Ge-Te and Cu-Te distances are almost equal to the corresponding interatomic distances in amorphous GCT [9].

We explained that this discrepancy originates from different length scales of the observations by XRD and XAFS [8]. The former measures a long-range and averaged periodicity of the lattice, and it is impossible to determine exact positions of atoms. Namely, the actual atoms are not guaranteed to be located at the lattice positions obtained by XRD. On the other hand, XAFS is able to directly determine local interatomic distances around the central atoms.

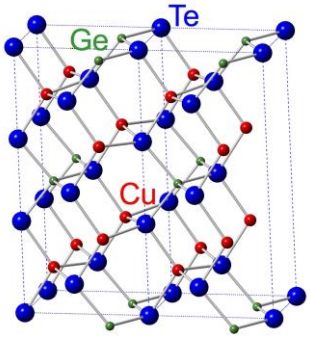

Fig. 1. (Color online) Crystal structure of GCT determined by XRD [7]. After [8].

Table 1. Comparison of the averaged R_{ij} in crystal GCT between the XRD [7] and XAFS [8] measurements together with R_{ij} in amorphous GCT obtained from a combination of XRD and XAFS [9].

	Crystal XRD [7]	Crystal XAFS [8]	Amorphous XRD& XAFS [9]
Ge-Te	2.51 (1)	2.60 (1)	2.61 (2)
Cu-Te	2.61 (1)	2.54 (1)	2.55 (3)

Besides the determinations of the local bond lengths, XAFS has a potential to obtain local atomic arrangements by using x-ray absorption near edge structure (XANES) very close to the absorption edge. In the previous structural results by Jóvári *et al.* [9], however, the XAFS data were only included in the reverse Monte Carlo (RMC) modeling procedure. Thus, the R_{ij} data given in Table 1 were not directly obtained from the XAFS measurements, but from a combination of the XAFS and diffraction results. Furthermore, they did not show the XANES spectra in their manuscript.

We have recently measure the XAFS spectra of amorphous GCT including the XANES ones to infill the lack of the above experimental information. In this paper, we show the XAFS results of amorphous GCT, which are directly compared with those of crystalline GCT [8] for discussing the phase change nature of the GCT alloys in a local structural sense.

2. Experimental procedure and data analysis

Amorphous GCT film samples with a thickness of 200 nm were deposited onto SiO_2(20 nm)/Si substrates at room temperature by radio-frequency sputtering of a polycrystalline GCT alloy target [6]. The base pressure of a vacuum chamber used for the sample preparation was below 4×10^{-5} Pa, and the radio-frequency power for the sputtering was 70 W [6]. Then, a crystalline GCT sample was obtained by annealing the amorphous sample at 250°C. The crystallinity of the crystalline sample was confirmed by XRD.

The XAFS experiments were carried out at the beamline BL12C of the Photon Factory in the High Energy Accelerator Research Organization (PF-KEK) in Tsukuba, Japan. XAFS data were measured at 30 K in fluorescence mode. X-rays emitting from a bending magnet source were monochromatized using a double Si(111) crystal. The incident x-ray intensity was measured using an ion chamber, and the fluorescent x-ray intensity from the sample was detected using a 19-channels pure Ge solid state detector.

The resultant XAFS functions were refined using a path expansion formalism as implanted in the REX2000 software package [10] in combination with FEFF6 program package [11]. A Fourier transform analysis was carried out for the XAFS oscillation functions $\chi(k)$ extracted from the raw absorption data. Then, the neighboring area of the Fourier transforms was inverse-Fourier transformed to obtain $\chi(k)$ concerning only the nearest neighbor atoms. Using a theoretical formula expressed as

$$\chi(k) = S_0^2 \sum_i \frac{N_i}{kR_i} F_i(k) \sin\left(2kR_i + \varphi_i(k)\right) e^{-\sigma_i^2 k^2},$$

fits were performed to obtain the coordination number N_i, distance R_i, and Debye-Waller factor σ_i of the neighboring atom i. Here, S_0^2 is the amplitude reduction factor, $F_i(k)$ the backscattering atomic form factor, and $\varphi_i(k)$ the phase shift.

3. Results and discussion

Fig. 2 shows the $k^2\chi(k)$ functions of (a) amorphous and (b) crystalline [8] GCT measured near the Ge K absorption edge. As shown in the figure, the amplitudes of these oscillations have two peaks at about 4.0 and 11.0 Å^{-1}. The existence of these two peaks in the amplitude is characteristic for a heavy element in the nearest-neighboring shell, i.e., the nearest-neighboring atoms are mainly composed of Te atoms.

Compared with the crystalline data in (b), the $k^2\chi(k)$ function of amorphous GCT in (b) is slightly small in amplitude and rather smeared out in the whole k range.

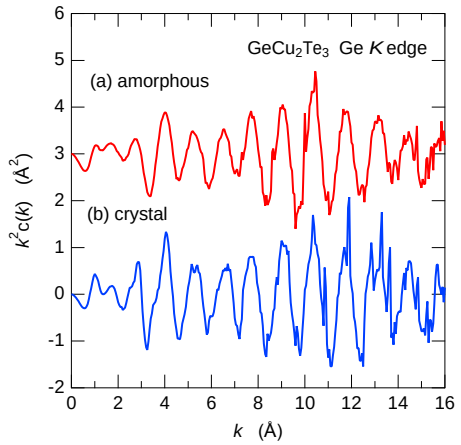

Fig. 2. (Color online)$k^2\chi(k)$ of (a) amorphous and (b) crystalline [8] GCT near the Ge K absorption edge.

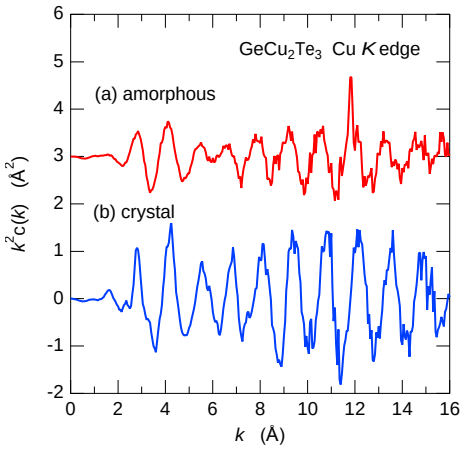

Fig. 3. (Color online) $k^2\chi(k)$ of (a) amorphous and (b) crystalline [8] GCT near the Cu K absorption edge.

Fig. 3 shows the $k^2\chi(k)$ functions of (a) amorphous and (b) crystalline [8] GCT measured near the Cu *K* absorption edge. As seen in the figure, overall trends near the Cu *K* edge are similar to those near Ge *K* edge shown in Fig. 2, i.e., two peaks in the amplitude in both the phase due to the Te nearest-neighbors, and the smaller amplitude and smeared-out oscillation in amorphous phase. Compared with the Ge *K* edge data, the damping of $k^2\chi(k)$ in the amorphous phase is much stronger, indicating a strong structural modification around the Cu atoms.

Circles in Fig. 4 show the Fourier transforms $|F(R)|$ of $k^2\chi(k)$ of (a) amorphous and (b) crystalline [8] GCT near the Ge *K* edge. As seen in the figure, the main peak height in the amorphous phase in (a) is lower than that in the crystalline phase in (b). The main peaks are located in both the phases at about 2.3 Å together with small peaks at about 2.0 Å. These peak features do not indicate the existence of two sites for the nearest-neighbor atoms but due to interferences of two peak features in the amplitudes of the $k^2\chi(k)$ functions. In addition, a relatively large peak is observed at about 3.8 Å in the crystalline GCT while that is mostly invisible in the amorphous phase. This difference is commonly seen in XAFS data of non-crystalline materials [12].

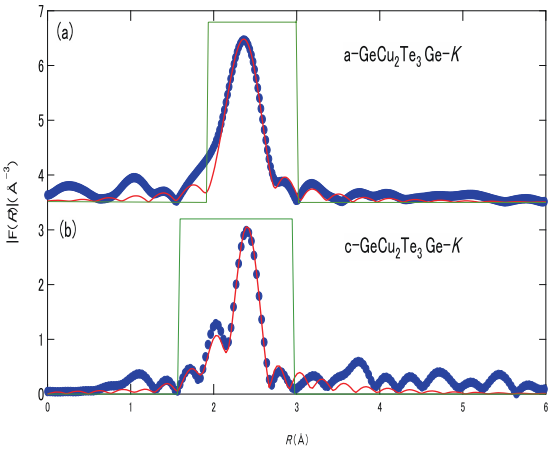

Fig. 4. (Color online) |F(R)| of (a) amorphous and (b) crystalline [8] GCT near the Ge K edge. Circes: Experimental data. Red curves: Fit functions by the theoretical analysis for the nearest-neighbors. Green curves Window functions for th e inverse - Fourier transforms.

Circles in Fig. 5 show the Fourier transforms $|F(R)|$ of $k^2\chi(k)$ of (a) amorphous and (b) crystalline [8] GCT near the Cu *K* edge. Mostly similar spectral features are observed in these spectra.

Then, we performed the theoretical fits for the nearest neighboring shells using window functions shown in green curves in Figs. 4 and 5. The $|F(R)|$ functions in these nearest-neighboring areas were inverse-Fourier transformed, and the results are shown by dots in Fig. 6 in order of (a) amorphous and (b) crystalline [8] GCT near the Ge *K* edge and (c) amorphous and (d) crystalline [8] GCT near the Cu *K* edge.

The red curves in Fig. 6 show the best fits of the theoretical calculations, which agree almost perfectly with the experimentally derived XAFS spectra. These fit functions were once more Fourier transformed and the results are correspondingly given as red curves in Figs. 4 and 5. These data are again in good agreement with the $|F(R)|$ functions in the nearest neighbor regions.

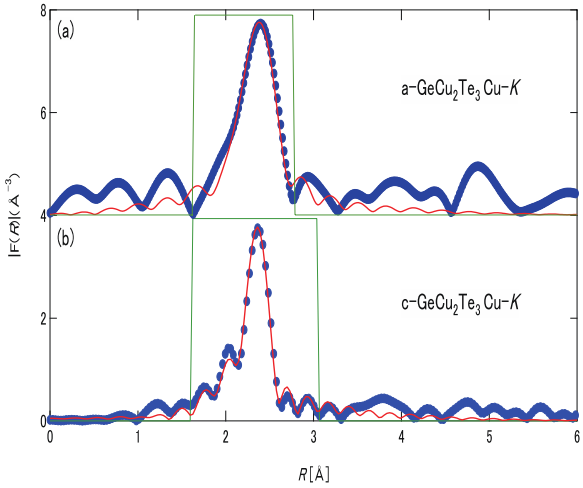

Fig. 5. (Color online) |F(R)| of (a) amorphous and (b) crystalline [8] GCT near the Cu K edge. Circes: Experimental data. Red curves: Fit functions by the theoretical analysis for the nearest-neighbors. Green curves: Window functions for the inverse-Fourier transforms.

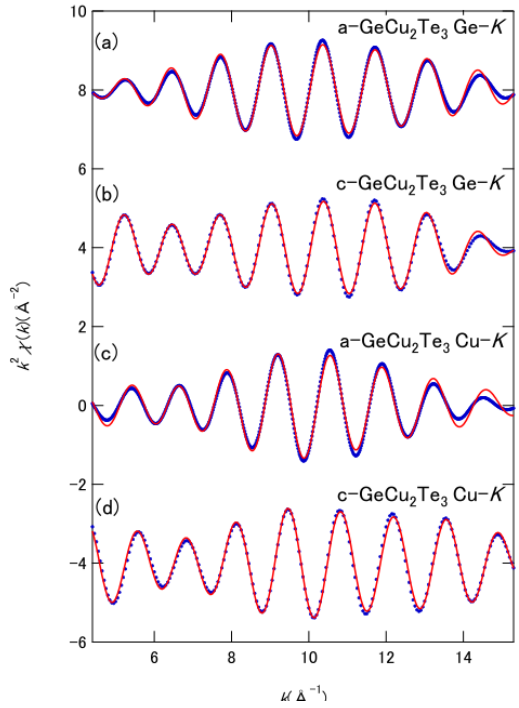

Fig. 6. (Color online) Inverse-Fourier transformed spectra of (a) amorphous and (b) crystalline [8] GCT near the Ge K edge and (c) amorphous and (d) crystalline [8] GCT near the Cu K edge. Dots: experimental data. Curves: the best fits.

Table 2 shows the partial coordination numbers N_{ij}, the partial nearest-neighbor distances R_{ij}, and the partial

Debye-Waller factors σ_i in crystal [8] and amorphous GCT. The suffix *ij* indicates the *j* neighboring atoms around the central *i* atom. The * mark indicates the fixed value for the analysis.

*Table 2. The N_{ij}, R_{ij}, and σ_i values in crystal [8] and amorphous GCT together with existing experimental data by Jóvári et al. [9] and ab initio MD simulation results by Skelton et al. [14]. * indicates the fixed value for the analysis.*

	i-j	N_{ij}	R_{ij} (Å)	σ_{ij} (Å)
Crystal [8]	Ge-Te1	2*	2.59	0.051
	Ge-Te2	2*	2.62	0.051
	Cu-Te2	2*	2.54	0.046
	Cu-Te2	1*	2.57	0.046
	Cu-Te3	1*	2.53	0.046
Amorphous [Present]	Ge-Ge	0*	–	–
	Ge-Cu	0.79	2.57	0.050
	Ge-Te	3.99	2.60	0.058
	Cu-Ge	0*	–	–
	Cu-Cu	2.44	2.60	0.065
	Cu-Te	1.85	2.58	0.064
Amorphous Experiment [9]	Ge-Ge	1.52(40)	2.48(2)	–
	Ge-Cu	0*	–	–
	Ge-Te	2.51(50)	2.61(2)	–
	Cu-Ge	0*	–	–
	Cu-Cu	2.20(40)	2.58(3)	–
	Cu-Te	1.86(30)	2.55(2)	–
Amorphous Theory [14]	Ge-Ge	0.12	2.96	–
	Ge-Cu	1.25	2.51	–
	Ge-Te	3.09	2.80	–
	Cu-Ge	0.62	2.51	–
	Cu-Cu	2.34	2.59	–
	Cu-Te	3.70	2.63	–

As reported in Ref. [8], discrepancies between the XAFS and XRD data in the crystal GCT were found in the averaged Ge-Te and Cu-Te interatomic distances, *i.e.,* the R_{GeTe} and R_{CuTe} values are respectively 2.61(1) and 2.54(1) Å obtained from the XAFS measurements [8], while smaller 2.51(1) and larger 2.61(1) Å from the XRD experiments [7].

We discussed why such an inconsistency occurs between the XRD and XAFS results even for the interatomic distances in crystalline GCT [8]. Fons *et al.* [13] suggested that diffraction is only sensitive to the averaged structure and insensitive to the local distortions, while the XAFS is able to directly determine local atomic positions around the central atom. According to their arguments, we explained the difference between the long-range periodicity and local structure for the Cu-Te bonds. If the Cu and Te atoms have positional fluctuations, the average positions of Cu and Te are located at the corresponding centers, which are observed by XRD. However, it is highly possible that the individual Cu-Te bond lengths are much shorter, which can be detected by XAFS. For this reason, XAFS measurements correctly determine the local interatomic distances rather than XRD. In the Ge-Te case, the longer bond lengths can be detected XAFS compared with XRD.

The structure of amorphous GCT was previously investigated by Jóvári *et al.* [9] using experimental results of XRD and XAFS combined with RMC simulations, and the results of N_{ij} and R_{ij} are given in Table 2. The total coordination numbers around the Ge and Cu are close to four as in the crystalline phase. However, there are significant fractions of homopolar Ge-Ge and Cu-Cu bonds in the amorphous phase. The R_{GeTe} and R_{CuTe} values in amorphous GCT obtained from previous experiments by Jóvári *et al.* [9] are 2.61(2) and 2.55(3) Å, respectively. It was very interesting that the averaged Ge-Te and Cu-Te interatomic distances in crystalline GCT obtained by our previous XAFS measurements are mostly equal to the above data [9]. It should be noted that the Ge-Cu correlations were artificially excluded in the first neighboring shells during the RMC modeling to avoid complex atomic configurations in amorphous GCT.

An *ab initio* molecular dynamics (MD) simulation was carried out by Skelton *et al.* [14] to investigate the structural and electronic natures of amorphous GCT, and the results of N_{ij} and R_{ij} are also given in Table 2. Compared with the above experimental data, several differences are realized. 1) A distinct value of $N_{GeCu} = 1.25$ is found, while the Ge-Ge homopolar bonds are negligible. 2) A larger number of $N_{CuTe} = 3.70$ is estimated, and the total coordination number around Cu reaches 6.76, much larger than the experimental value of fourfold coordinated. 3) Although it is consistent that $R_{GeTe} = 2.80$ Å is larger than $R_{CuTe} = 2.63$ Å, both the values are larger than the experimental values of 2.61 and 2.58 Å, respectively.

For our XAFS analysis near the Ge *K* edge, we firstly allowed only the existence of the Ge-Ge correlations in addition to the usual Ge-Te bonds by following the previous experimental data. However, the fit results were not satisfied by comparing with the second trial with allowing only a large number of the Ge-Cu correlations as the theory suggested. For the analysis near the Cu *K* edge, we excluded the Cu-Ge bonds as the previous experiment was set for the analysis to avoid the effect from the small number of Cu-Ge correlation. The theoretical result of the small value $N_{CuGe} = 0.62$ also supported this hypothesis.

Our present XAFS results are also tabulated in Table 2. Although the present data are obtained purely from the XAFS experiments, the obtained R_{GeTe} value of 2.60 Å in amorphous GCT is in good agreement with the mixed data of XRD and XAFS [9], 2.61 Å, and R_{CuTe} of 2.58 Å is slightly larger than the previous value of 2.55 Å [9]. It was confirmed that these values evaluated from the theory, 2.80 and 2.63 Å [14] are larger than the experimental data beyond the experimental errors.

As regards the coordination numbers, the present N_{GeTe} value is mostly fourfold as is in the crystalline phase. However, additional Cu neighbors of ~0.8 are included in the first neighboring shell around the Ge atoms. The total coordination number around the Ge atoms is ~4.8, which is slightly larger than the 8–*N* rule that both the previous experiment [9] and theory [14] obtained.

Around the Cu atoms, however, the N_{CuTe} value is only 1.85, which is much smaller than the fourfold crystalline value. This result is in good agreement with the previous experimental value of 1.86 [9], but both the

experimental results are much smaller than the theoretical value of 3.70, similar to the crystalline value of 4. We obtained the large value of N_{CuCu} = 2.44, which is close to the previous experiment of 2.20 [9] and theory of 2.34 [14]. The total coordination number around the Cu atoms is ~4.3. Thus, it is concluded from the present XAFS measurements that the atomic configurations around the Ge atoms are a small modification of the crystalline one, while those around the Cu atoms are quite different and the Cu-Cu homopolar coordination become an important role in the amorphous phase.

On the amorphization, the σ_{ij} values of the Ge-Te and Cu-Te correlations increase due to the increase of static positional fluctuations in the amorphous phase. It should be noted that on the amorphization, σ_{GeTe} increases by only ~14% while σ_{CuTe} by ~40%. As a result, $\sigma_{GeTe} > \sigma_{CuTe}$ in the crystalline phase, while $\sigma_{GeTe} < \sigma_{CuTe}$ in the amorphous phase, suggesting that the atomic configurations around the Cu atoms become much fluctuated in the radial direction on the crystalline-amorphous phase transition.

It is well-known that the XANES spectra are very sensitive for three-dimensional atomic configurations around the edge element. Fig. 7 shows the XANES spectra of GCT near the (a) Ge and (b) Cu *K* absorption edges. Upper and lower curves indicate those for the amorphous and crystalline phases, respectively. The spectra were normalized to the jump at the absorption edges.

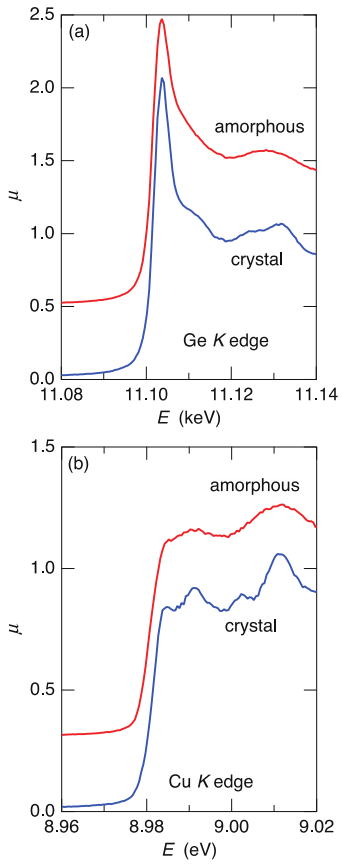

Fig. 7. (Color online) XANES spectra of GCT near the (a) Ge and (b) Cu K absorption edges. Upper: amorphous, lower: crystal.

As usual, the XANES spectrum of amorphous GCT near the Ge *K* edge shows small damping features from the crystalline spectrum. These trends may be originated from the preservation of fourfold coordinated configuration around the Ge atoms even though one of the four neighboring Te atoms in the crystal GCT is replaced by a Cu atom in the amorphous GCT.

On the other hand, an extremely damped feature is observed in the XANES spectrum of amorphous GCT near the Cu *K* edge, which corresponds to the large change in the local coordinations around the Cu atoms obtained by the present XAFS measurements.

These XAFS data on amorphous GCT can be utilized for a RMC modeling in combination with anomalous x-ray scattering results, which is now in progress.

4. Summary

The structure of crystalline and amorphous GCT phase change material was investigated by XAFS. The averaged interatomic distances of Ge-Te and Cu-Te in the crystal phase are confirmed to contradict the x-ray diffraction data, and are mostly equal to the experimental data in the amorphous phase. As regards the coordination numbers, the atomic configurations around the Ge atoms are a small modification of the crystalline one, while those around the Cu atoms are quite different and the large number of the Cu-Cu homopolar coordination become an important role in the amorphous phase. The XANES data near the Ge *K* edge show a similarity of the local atomic configurations around the Ge atoms between the crystalline and amorphous $GeCu_2Te_3$. However, those near the Cu *K* edge indicate a large smearing-out on the amorphization, corresponding the large differences in the atomic configurations around the Cu atoms.

Acknowledgments

The authors acknowledge Prof. F. Ichikawa of Kumamoto University for the support of XRD measurements on the thin film samples. The XAFS experiments were carried out at BL12C of PF-KEK (Proposal Nos. 2010G559 and 2012G522). This work was partially supported by JSPS Grant-in-Aid for Scientific Research on Innovative Areas ‘3D Active-Site Science’ (No. 26105006).

References

[1] M. Wuttig N. Yamada, Nature Mater. **6**, 824 (2007).
[2] S. Raoux, M. Wuttig (ed.), Phase Change Materials (Springer-Verlag, New York, 2008.
[3] N. Yamada, E. Ohno, K. Nishiuchi, N. Akahira, M. Takao, J. Appl. Phys. **69**, 2849 (1991).
[4] Y. Sutou, T. Kamada, M. Sumiya, Y. Saito, J. Koike, Acta Mater. **60**, 872 (2012).
[5] Y. Sutou, Y. Saito, J. Koike, P. Jóvári, I. Kaban, E\PCOS2012 **S3**-04 (2012).
[6] T. Kamada, Y. Sutou, M. Sumiya, Y. Saito, J. Koike, Thin Solid Films **520**, 4389 (2012).

[7] G. E. Delgado, A. J. Mora, M. Pirela, A. Velásquez-Velásquez, M. Villarreal, B. J. Fernández, Phys. Status Solidi A **201**, 2900 (2004).
[8] K. Kamimura, K. Kimura, S. Hosokawa, N. Happo, H. Ikemoto, Y. Sutou, S. Shindo, Y. Saito, J. Koike, Z. Phys. Chem., 2015-0672.
[9] P. Jóvári, Y. Sutou, I. Kaban, Y. Saito, J. Koike, Scr. Mater. **68**, 122 (2013).
[10] T. Taguchi, T. Ozawa, H. Yashiro, Phys. Scr. T**115**, 205 (2005).
[11] S. I. Zabinsky, J. J. Rehr, A. Ankudinov, R. C. Albers, M. J. Eller, Phys. Rev. B **52**, 2995 (1995).
[12] F. Evangelisti, M. G. Proietti, A. Balzarotti, F. Comin, L. Incoccia, S. Mobilio, Solid State Commun. **37**, 413 (1981).
[13] P. Fons, A. V. Kolobov, M. Krbal, J. Tominaga, K. S. Andrikopoulos, S. N. Yannopoulos, G. A. Voyiantzis, T. Uruga, Phys. Rev. B **82**, 155209 (2010).
[14] J. M. Skelton, K. Kobayashi, Y. Sutou, S. R. Elliott, Appl. Phys. Lett. **102**, 224105 (2013).

*Corresponding author: hosokawa@sci.kumamoto-u.ac.jp